ADVANCED OPTICAL MATERIALS
www.advopticalmat.de

Finite Size Effects on Light Propagation throughout Random Media: Relation between Optical Properties and Scattering Event Statistics

José M. Miranda-Muñoz, Victoria Esteso, Alberto Jiménez-Solano, Gabriel Lozano, and Hernán Míguez**

This work introduces a thorough analysis of light transport in thin optically disordered media. The diffusive properties of a turbid material are generally dictated by the transport mean free path, l_t. For depths larger than this characteristic length, light propagation can be considered fully randomized. There is however a range of thicknesses for which light becomes only partly randomized, as it only undergoes a single or very few scattering events. The effects of such finitude are experimentally and theoretically studied on the optical properties of the material, such as the angular distribution of scattered light. Simulations provide insight into the phenomena that occur within the optically disordered slab, like the number of scattering events that photons undergo during propagation throughout the material, as a function of the built-in wavelength dependent scattering mean free path, l_{sc}. This approach provides fundamental information about photon transport in finite optically random media, which can be put into practice to design diffusers with specific requirements in terms of the spectral and angular properties of the scattered light.

The description of light transport in optically random media is a challenging task, since the phase and the direction of the propagating electromagnetic waves are randomized in an intricate manner.[1–12] Optical disorder in nonabsorbing media generally produces successive elastic scattering of light, triggering diffuse propagation of waves. This phenomenon causes broadband reflection and transmission in the material, which endow it with a white opacity.[13] Whiteness and opacity are therefore dependent on the number of scattering events and, thus, thickness of the material. In this regard, different synthetic approaches have been taken to achieve materials in which diffuse light propagation can be controlled, leading to the development of different types of photonic glasses.[14–18] At the same time, efforts have been devoted to structures optimizing light-scattering for the fabrication of highly efficient Lambertian-like reflectors.[19–24] These approaches seek the development of highly opaque and white materials in which optical scattering is maximized for the thinnest possible system, thus minimizing material use. These materials would have special interest for the fabrication of commercial products designed to exhibit a white appearance, such as the manufacture of paper.[25] In this kind of application, the high scattering strength of the material ensures multiple scattering and randomization of the propagating light, enabling the definition of the transport mean free path, l_t, i.e., the average distance over which the propagation direction of the light wave can be considered randomized and information on its original incoming trajectory is lost. Less effort has been focused on media for which limited thickness precludes light from total randomization and propagation occurs in the single or few scattering events regime.[26,27] Here, ballistic transmittance prevails over diffuse transport and the scattering properties of the materials are described by means of the scattering mean free path, l_{sc}, i.e., the average distance a photon travels between two scattering events. Besides, whereas the intensity of light emerging from a perfect diffuser exhibits a Lambertian profile, fully isotropic, the intensity of the light exiting a thin slab describes an angle-dependent distribution that is progressively modified with the number of scattering events, that is, either the value of l_{sc} or the thickness of the slab.

We discuss herein finite-size effects in random media. We present a combined experimental and theoretical analysis of the thickness-dependent evolution of the optical response of an optically random medium before multiple scattering fully determines light transport and complete randomization occurs. In order to gain a deeper insight into the characteristics of the optical response experimentally observed, we employed a theoretical approach based on a Monte Carlo method combined with Mie theory to simulate the angular distribution of

J. M. Miranda-Muñoz, V. Esteso, Dr. A. Jiménez-Solano,[+] Dr. G. Lozano, Prof. H. Míguez
Multifunctional Optical Materials Group
Institute of Materials Science of Sevilla
Consejo Superior de Investigaciones Científicas – Universidad de Sevilla (CSIC-US)
Américo Vespucio 49, 41092 Sevilla, Spain
E-mail: g.lozano@csic.es; h.miguez@csic.es

The ORCID identification number(s) for the author(s) of this article can be found under https://doi.org/10.1002/adom.201901196.

[+]Present address: Max Planck Institute for Solid State Research, Heisenbergstrasse 1, 70 569 Stuttgart, Germany

DOI: 10.1002/adom.201901196

light scattered by a Mie glass for increasing thickness in order to examine the effects of finitude on the diffuse propagation of light. Our model allows to study the effects of the finite-size of random media not only by analyzing the angular distribution of the light scattered by a slab of an optically random medium, but also by keeping track of the characteristics of each photon during its trajectory, such as its exit direction or the number of scattering events it undergoes before leaving the material. Thus aspects of light transport in random media not accessible through experimental procedures are revealed. Furthermore, our approach provides a means to devise a diffuser with controlled opacity in which the angular distribution of transmitted and reflected light can be controlled.

Nonabsorbing optically random media presenting strong scattering are known to induce a diffuse transport of the light, displaying a white appearance typical of turbid media due to multiple scattering of the light. For system size, L, verifying the condition $\lambda << l_t << L$, where λ refers to the wavelength of the incident beam, light propagates as defined by the diffuse regime, as schematized in **Figure 1**a. In this regime, the light emerging from the material exclusively propagates in a diffusive manner as a consequence of full randomization and its angular distribution obeys Lambert's cosine law. This is illustrated in the inset of Figure 1a for the case of a squared piece of paper, which behaves as a perfect diffuser. Its high opacity, derived from numberless scattering events, prevents observation of the light source through it. If the thickness of the system is reduced below l_t, the diffuse regime condition does not hold anymore and a different approach is therefore required for the description of light transport. In this situation, a fraction of the out-coming intensity is ballistically transmitted, as drawn in Figure 1b, which gains relevance as thickness becomes shorter. This is evidenced in the inset of Figure 1b, where light propagates through a thin slab of a scattering material, even allowing, to a great extent, observation of the light source behind the film. In this regime of single or few scattering events in which l_t cannot account for the propagation of light in terms of the transmitted light, the diffuse properties of the material can be described based on the scattering mean free path, l_{sc}. The random medium under consideration corresponds to a system structured as a Mie glass.[18] Specifically, the material consists of a solid mesoporous transparent anatase matrix embedding randomly distributed quasi-monodisperse polycrystalline TiO_2 spheres of a few hundred nanometer radius surrounded by a hollow shell, as illustrated in Figure 1c. Figure 1d shows an image of the cross-section of the structure experimentally realized, attained by field emission scanning electron microscopy (FESEM).

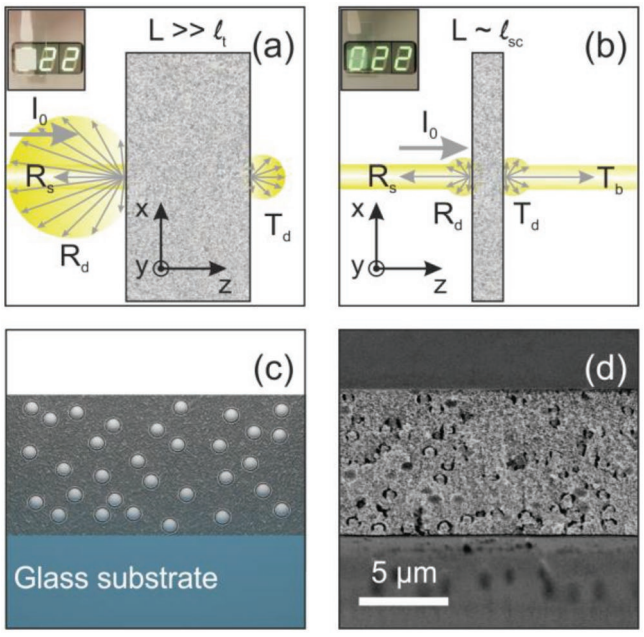

Figure 1. Illustration of the propagation of light throughout an optically random medium a) in the diffuse regime and b) in a regime of weak scattering. Examples of materials yielding light propagation in either regime are included as insets. I_0 corresponds to the intensity of the incident beam, R_s and T_b refer to the specular reflectance at the air–Mie glass interface and the ballistic transmittance exiting the material, respectively, and R_d and T_d to their corresponding diffuse components, all of them determined with respect to I_0. c) Schematic of the system under consideration displaying its constituents. d) Scanning electron microscopy cross-section image of the experimental optically disordered medium comprising a mesoporous anatase matrix integrating monodisperse crystalline TiO_2 spheres surrounded by an air shell as scattering structures.

In order to analyze the influence of finite-size effects on light transport in optically random media, we determined the spectral and angular optical response of three thin slabs (L = 9 μm) presenting different l_{sc} values. The l_{sc} values of the materials were controlled through the radius, r, and volume filling fraction, f, of the scattering inclusions. Namely, the set of values chosen for those parameters were (r = 95 ± 20 nm, f = 5%), (r = 225 ± 20 nm, f = 5%) and (225 ± 20 nm, f = 10%), which determine l_{sc} of 6.5, 1.8, and 0.9 μm, respectively, at λ = 600 nm, according to Mie formalism. For this wavelength, negligible contributions from absorption of the optical material are expected. The ballistic transmittance spectra yielded by these films are displayed in **Figure 2**a. As expected, for a fixed value of the slab thickness, a decrease of l_{sc} results in a lower fraction of ballistically transmitted light. Specifically, a change in the l_{sc} value from 6.5 to 1.8 μm causes a decrease of T_b from 29% to 6% at λ = 600 nm, and a further decrease to 3% for the shortest l_{sc} considered, 0.9 μm. Reducing l_{sc} entails an increase of scattering events along the same length, generally increasing the fraction of light diffusively propagated at the expense of ballistic transmittance, as corroborated by Figure 2b. With the purpose of understanding the influence of the specific characteristics of the dispersion of inclusions on the eventual angular distribution of transmitted light, we employed a double goniometer coupled to a spectrophotometer (Cary 7000 Universal Measurement Spectrophotometer, Agilent Technologies) to measure the light emerging at different angles for each system when the incident beam impinges normally to the surface of the disordered slab. Results attained for radiation of λ = 600 nm are plotted in Figure 2c, in polar graphs, where 0° and 180° correspond, respectively, to ballistically transmitted and back reflected light. The effect of shortening l_{sc} is evidenced by the broadening of the angular distribution of both transmitted and reflected light intensities: the increase of scattering events modifies the angular pattern, which approaches that of a Lambertian emitter as the material becomes gradually more diffusive. The effect of

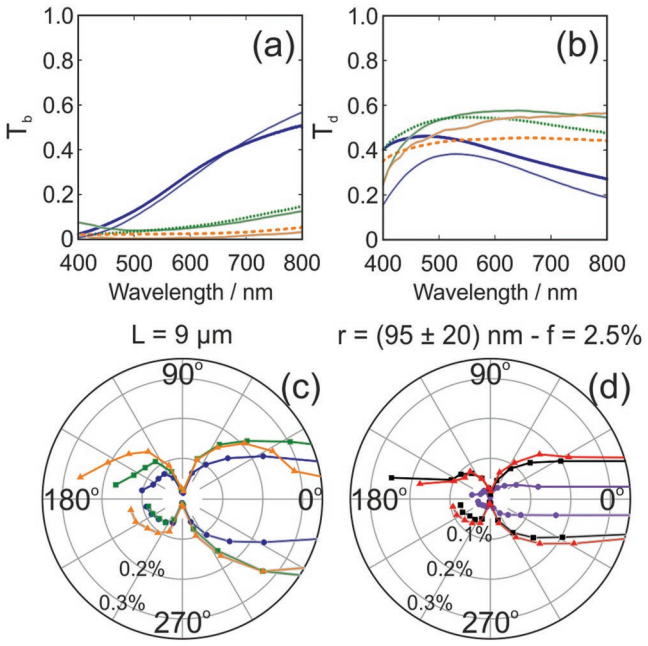

Figure 2. Verification of the optical model through comparison with experimental data. Experimental (thick lines) and calculated (thin lines) a) ballistic and b) diffuse transmittance yielded by films with the scattering centre conditions $r = 95 \pm 20$ nm, $f = 5\%$ (blue solid line), $r = 225 \pm 20$ nm, $f = 5\%$ (green dotted line) and $r = 225 \pm 20$ nm, $f = 10\%$ (orange dashed line) and thickness $L = 9$ µm. c) Angular distribution of the light scattered by the systems presented in panels (a) and (b) at $\lambda = 600$ nm, with the scattering centre conditions $r = 95 \pm 20$ nm, $f = 5\%$ (blue-dot line), $r = 225 \pm 20$ nm, $f = 5\%$ (green-square line) and $r = 225 \pm 20$ nm, $f = 10\%$ (orange-triangle line) and thickness $L = 9$ µm. Calculations consider $r = 95 \pm 20$ nm, $f = 2.5\%$ (blue-dot line), $r = 225 \pm 20$ nm, $f = 2.5\%$ (green-square line) for 9-µm-thick slabs and $r = 225 \pm 20$ nm, $f = 5\%$ (orange-triangle line) for a 8-µm-thick slab, respectively. d) Angular distribution of the light scattered by a system with the scattering centre condition $r = 95 \pm 20$ nm, $f = 5\%$, and thickness $L = 1.84 \pm 0.07$ µm (violet-dot line), 6.59 ± 0.18 µm (black-square line), and 9.3 ± 0.3 µm (red-triangle line) at $\lambda = 600$ nm. Calculations consider the scattering centre conditions $r = 95$ nm, $f = 2.5\%$. In the angular representations, the curves in the upper half correspond to the experimental data, in which each dot is associated to a measured value, whereas the lines in the lower half refer to the simulated data. Light impinges on the system from the left side.

varying thickness was analyzed for the case of a slab yielding $l_{sc} = 6.5$ µm, corresponding to the sample characterized by the experimental conditions ($r = 95 \pm 20$ nm, $f = 5\%$), which is an intermediate value compared to the range of thickness available. The angular distributions displayed in Figure 2d for slabs of thickness 1.84 ± 0.07, 6.59 ± 0.18, and 9.3 ± 0.3 µm reveal that the trend expected for increasing values of the thickness is in fact similar to that corresponding to an increment of scattering strength, as the average scattering event number escalates with both parameters.

In order to gain a deeper insight into these trends, we obtained the theoretical spectral and angular optical response of these systems by using a 3D model previously reported by some of us, in which Mie scattering theory and a statistical Monte Carlo approach are combined for the determination of the trajectory of individual photons in any layered system.[28] In order to highlight the 3D nature of the model, a 3D representation of the trajectory of a photon undergoing several scattering events throughout a Mie glass is available in Figure S1 in the Supporting Information. Such model has been successfully used in the past to describe optically disordered dye-sensitized solar cells or other Mie glasses. Although the light is herein considered to impinge on the Mie glass from the free air, our model is also able to generate the photons inside the material if necessary for the simulation of an active material presenting photoluminescence. In fact, simulations of this sort were performed for a solar concentrator integrating photonic crystals designed and characterized in a previous publication.[29] The spectra and angular distributions derived from the calculations have been included in Figure 2 for the sake of comparison (lines in the lower half of the polar plots, same color code as the experimental curves depicted in the same figure). The spectral refractive index employed as input data in the calculations have been included in Figure S2 in the Supporting Information. Size and concentration of scattering centers were chosen within the experimental uncertainty with respect to nominal experimental values. A size dispersion of ≈20 nm around the average size of the TiO_2 inclusions has been considered in the calculations, in agreement with the estimation of particle size performed from electron microscope images. Furthermore, also in agreement with our experimental observations, our model takes into account the presence of an air layer surrounding the scattering centers. The presence of such shell does not alter significantly the optical response of the scatterers for the specific material under consideration as l_{sc} calculations reveal (please see Figure S3 in the Supporting Information). The adequacy of the model to reproduce qualitatively and quantitatively, to a great extent, the experimental trends observed both spectrally (Figure 2a,b) and angularly (Figure 2c,d) indicates that the optically disordered thin films herein investigated can be described without taking into account phase correlation effects. In other words, the total scattering of the ensemble can be understood by considering only a series of consecutive individual scattering events, each one giving rise to an angular distribution of scattered light governed by Mie theory. Based on this agreement, in what follows we make use of this model to analyze in more detail the origin of the observed angular distribution of diffuse light transmitted and reflected by thin films.

We theoretically analyzed the angular distribution of scattered light intensity yielded by slabs of different thicknesses and their relationship with the distribution of scattering events light undergoes. The structural parameters of the simulated film are $r = 225$ nm — $f = 2.5\%$, for which $l_{sc} = 3.6$ µm and $l_t = 15$ µm, estimated at $\lambda = 600$ nm, using the expressions

$$l_{sc} = \left(\rho \cdot \sigma_{sc}\right)^{-1} \quad (1)$$

$$l_t = \frac{l_{sc}}{1 - \langle \cos\theta \rangle} \quad (2)$$

in which ρ is the particle number density, σ_{sc} the scattering cross section of a single particle and $\langle \cos\theta \rangle$ is the average of the cosine of the scattering angle θ weighted by the relative scattered intensity at that angle, both calculated according to Mie formalism.[28] From a different perspective, our Monte Carlo simulation[18] allows us studying the calculated total transmittance spectra from slabs of diverse thicknesses, and gives us an independent estimation of the transport mean

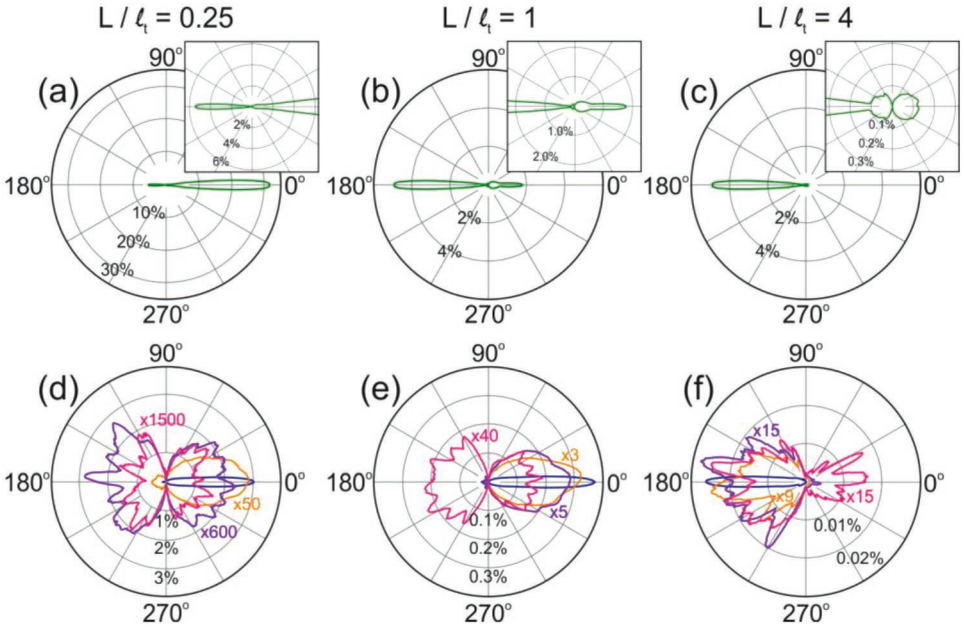

Figure 3. a–c) Angular distribution of the light scattered at $\lambda = 600$ nm by the simulated system for scattering centre dispersion parameters $r = 225$ nm, $f = 2.5\%$, and thickness $L = 0.25l_t$, $L = 1l_t$ and $L = 4l_t$, respectively. The insets display a zoom-in of the corresponding angular distribution of each panel. d–f) Angular distributions of the photons scattered $s = 1$ (blue), 3 (orange), 5 (violet), and 10 (pink) times at $\lambda = 600$ nm by systems of thickness $L = 0.25l_t$, $L = 1l_t$ and $L = 4l_t$, respectively. The magnification of the scale has been duly indicated when required.

free path value of $l_t = 10$ µm at $\lambda = 600$ nm, which is of the same order than the value $l_t = 15$ µm determined from Mie formalism. As mentioned above, diffuse propagation in a random material is set by the condition $L >> l_t$, a limit in which light propagation is governed by multiple scattering. We theoretically inspected slabs of thicknesses from $L < l_t$ up to $L = 4l_t$, a range for which the optical response should evolve from being strongly determined by the finite size of the slab to showing the characteristic features of a fully developed disordered "bulk" material. For short thickness values, e.g., $L = 0.25l_t$, photons undergo only a few scattering events and, as a consequence, an important fraction of the incident light does not deviate from the incident beam and emerges as T_b, as shown in **Figure 3**a, where around 32% of the light is ballistically transmitted. For a thicker slab, $L = 1l_t$, light is granted multiple chances to be scattered, thus resulting in a higher fraction of light propagating diffusively at the expense of T_b, which is significantly reduced to an exiguous 1.8% when compared to the previous case, as it can be seen in Figure 3b. The outcome of such sharp decrease of the total transmittance is the appearance of the whitish opacity typical of random media. Furthermore, in opposition to a slab of thickness $L = 0.25l_t$, the angular distribution of the transmitted light presents a fairly isotropic shape, resembling a Lambertian diffuser, as a consequence of a significant fraction of light propagating diffusively. Eventually, for slab thicknesses much larger than l_t, e.g., $L = 4l_t$, most of the incident light is diffusively reflected. Light is scattered numberless times, which hampers transmittance, therefore resulting in high opacity, as shown in Figure 3c. Besides, the perfectly isotropic angular pattern described by the transmitted intensity reveals full randomization of the light. As for the reflected light, its predominance in the angular distribution derives from the presence of an interface at the entrance of the system, so that a fraction of the incident light is specularly reflected and not coupled into the material. This point is further discussed in Figure S4 in the Supporting Information. Whereas light ballistically transmitted is highly affected by the irregular variations the refractive index in the material, under the assumptions we are considering, and in good agreement with the experimental results, the specular reflectance is largely dictated by the refractive index contrast between the material under consideration and the surrounding medium, which becomes evident when observing the evolution of the R_s value for increasing thickness, namely, 5.4%, 4.9%, and 4.9% for $L = 0.25l_t$, $L = 1l_t$, and $L = 4l_t$, respectively. For short enough thicknesses of the slab, photons reflected at the second interface and exiting the material in the backward direction without undergoing a scattering event contribute to R_s. As thickness increases, the probability of photons crossing the slab twice without resulting scattered decreases, thus reducing the value of R_s up to 4.9%, defined exclusively by photons scattered at the entrance interface due to the refractive index contrast. Information on the evolution of R_s in relation to the thickness of the slab is available in Figure S5 in the Supporting Information. This point is addressed again below when analyzing the fraction of nonscattered photons depending on the slab thickness. The total angular distributions displayed in Figure 3a–c can be visualized as the sum of contributions of the angular patterns described by light scattered a specific number of times. Indeed, Figure 3d–f shows specific cases for the thickness values under consideration. When neglecting the nonscattered photons, the main contribution to the total angular distribution for $L = 0.25l_t$ derives from the number of photons scattered just once, as evidenced when comparing Figure 3d,a. Due to Mie scattering, the angular distribution of these photons preserve to a high extent the typical forward-oriented shape characteristic of this type of scattering. The low

probability that photons undergo a large number of scattering events in systems with such thickness causes higher contributions to play a small part in the total intensity, as revealed by the high magnifications required in Figure 3d for the visualization of the angular patterns of higher contributions. For a thicker slab, the contribution by photons scattered more than once start becoming significant, as revealed by the lower magnification values required in Figure 3e. Throughout a slab of thickness $L = 1l_t$, not only is it likely that photons are scattered three or five times, but these can also reach the end interface and exit the system, therefore generating angular distributions for photons undergoing as many scattering events exhibiting a strong transmitted component, especially noticeable when comparing to the respective distributions in Figure 3d. As film thickness increases, the probability of photons undergoing a higher number of scattering events rises and the angular distribution of light broadens, as shown in Figure 3b, which is an indication of the partial randomization of propagating light. Eventually, if the thickness is considerably large, such as for the case $L = 4l_t$, photons undergoing one scattering event can only be detected in the backward direction, since those photons scattered in the forward direction will most likely undergo further scattering events before exiting the slab in transmission, see Figure 3f. Let us notice that photons undergoing three and five scattering events still predominantly exit the slab in the backward direction, that is, as reflected light. The fact that similar magnifications were required for the visualization of the distributions corresponding to photons scattered three, five, and ten times reveals that in this limit the weight of the higher order contributions decreases slowly. Subsequently, the small fraction of transmitted light exhibited by the total angular distribution is fully randomized. Data of the angular distribution of the scattered light for a thin slab of thickness $L = l_{sc}$, where a single scattering event is most likely, are available in Figure S6 in the Supporting Information.

Further insight into these trends is provided by the histograms displayed in **Figure 4**a–c that illustrate all the photons emerging from the material, either reflected or transmitted, in terms of the number of scattering events they underwent for the three considered L/l_t values. It should be mentioned that, although reflection at any of the surfaces of the system would technically involve a scattering event according to its definition as any phenomenon removing photons from the incident beam, specularly reflected photons at both front or rear interfaces are herein considered nonscattered photons. Indeed, only modifications of the trajectory of the photons caused from interactions with the spherical inclusions are regarded as scattering events in the model. Under these premises, the most likely number of scattering events increases with film thickness, as shown in Figure 4. In the histograms, the contribution of photons specularly reflected has been omitted. In comparison to a system of thickness $0.25l_t$, Figure 4a, the probability of photons undergoing one single scattering event is reduced when increasing the size of the system to $L = 1l_t$, as displayed in Figure 4b. When the material exhibits a behavior resembling that of a perfect diffuser, i.e., for $L = 4l_t$, a most probable number of events can still be distinguished, as shown in Figure 4c, although its value is less prominent than for thinner films. In fact, as the disordered materials become larger, the probability curve flattens, as it can

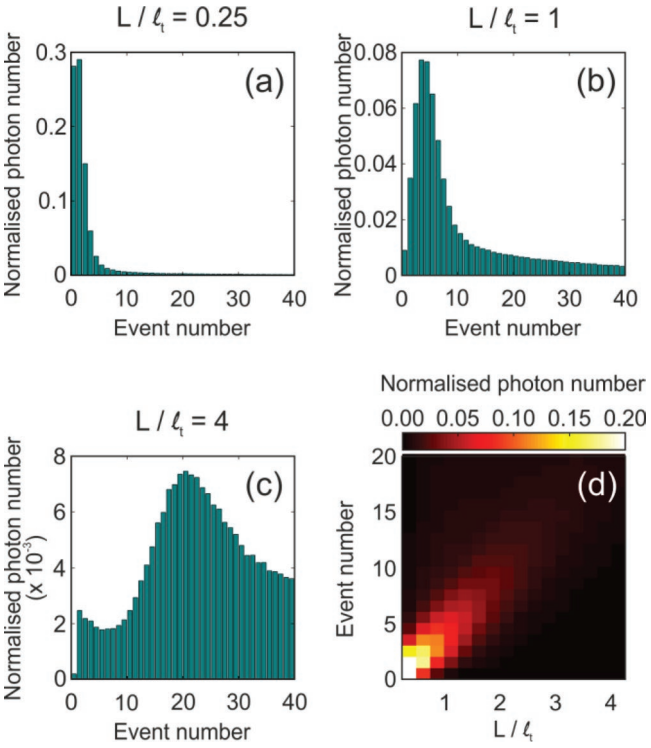

Figure 4. a–c) Histograms of the normalized number of scattered photons in relation to the number of scattering events they underwent at $\lambda = 600$ nm for systems with thickness values $L = 0.25l_t$, $L = 1l_t$, and $L = 4l_t$, respectively. d) Normalized number of photons scattered by the simulated system with scattering centre conditions $r = 225$ nm, $f = 2.5\%$, at $\lambda = 600$ nm in relation to the number of undergone scattering events and its thickness in l_t units. For the sake of clarity, specularly reflected photons have been omitted in this representation.

be readily seen in Figure 4d, in which a color map illustrating the evolution of the distribution of photons for different values of L/l_t according to the number of undergone scattering events is shown. The histogram corresponding to a thin slab of thickness $L = l_{sc}$, a case of interest for which one single scattering event is most likely, has been included in Figure S7 in the Supporting Information.

In summary, this work poses a new perspective on how to deal with the transport of light in optically random media of thicknesses for which the classic picture of diffusive transport fails. Experimentally, we use mesoporous anatase films integrating a random distribution of monodisperse crystalline TiO_2 spheres as a platform for our study, determining the spectral and angular optical response of samples with different thickness as well as concentration and size of scatterers. Theoretically, we develop an optical model based on a combination of Monte Carlo with Mie formalism that enabled reproduction of the trends experimentally observed, and allowed us achieving a deeper insight into the statistics of the photon scattering events taking place within the material. We were able to examine the evolution of the angular distribution of the scattered light for increasing thickness of the slab, from conditions under which photons are scattered a few times, to those for which a high fraction of the light propagates diffusively, and light transport becomes randomized. This analysis provided information on

the progressive change of the shape of the angular pattern when increasing the number of scattering events. These results could therefore help understanding fundamental aspects of light transport in finite size turbid media and hence devising diffusers with specific spectral and angular optical response.

Experimental Section

Modeling: The propagation of light was simulated according to an upgraded version of a theoretical method already reported.[28] The model essentially consists in a Monte Carlo approach combined with Mie theory, so that the trajectory of a photon entering a multilayer system comprising any number of layers with any number of components can be traced. When extended to a larger number of photons, the model allows collection of the emerging photons and thus determination of magnitudes, such as reflectance, transmittance, and the absorptance at each layer, as well as the exit angle of each photon. Furthermore, due to the ray-tracing nature of the model, it allows the analysis of specific properties of the emerging photons, such as the number of scattering events undergone by every photon exiting the system, thus enabling novel representations, such as the angular pattern of photons exiting the system after undergoing a specific number of scattering events. A 100 nm thick layer of a constant refractive index $n = 1.35$ was considered on top of the Mie glass in order to increase the coupling of light into the material. This was necessary to compensate for the effect of the light specularly reflected by the porous TiO_2 matrix experimentally observed and not accounted for in the model. The filling fraction was defined as the ratio of the total volume occupied by the scattering centers to the volume of the film and it considered the air shell surrounding the particle. For the generation of the angular patterns, a detector presenting a solid angle spanning over 14° and a Gaussian response was simulated, so that 100% the photons were collected at the centre of the detector, that is, 0°, and 50% at angles ±3°.

Material Fabrication: The Mie glasses whose optical response was determined for the present study were fabricated according to a solution-processing based procedure reported elsewhere.[18]

Optical Characterization: Angle-dependent measurements of light exiting the materials were performed through a UV–vis–NIR spectrophotometer (Cary 5000, Agilent Technologies) coupled to the Universal Measurement Accessory, UMA, which allows collection of photons around the sample in a plane perpendicular to it by means of a detector with a solid angle spanning over 14°. Determination of the spectral magnitudes in Figure 2 was enabled through the Internal Diffuse Reflectance accessory, which consists in an integrating sphere. This accessory enabled the determination of the intensity collected inside the sphere after crossing the slab (total transmittance, T), and the determination of T_d by allowing the ballistic component to escape the sphere through a port placed on the other side opposite the entrance port. T_b is derived from these two magnitudes employing $T_b = T - T_d$.

Structural Characterization: Values of the thickness of the slabs were extracted from cross-section images generated by means of a scanning electron microscope (S-4800, Hitachi). The considered thickness values are derived from averaging those determined from images taken on different regions of the sample.

Supporting Information

Supporting Information is available from the Wiley Online Library or from the author.

Acknowledgements

This project has received funding from the Spanish Ministry of Economy and Competitiveness under grant MAT2017-88584-R and from the European Research Council (ERC) under the European Union's Horizon 2020 Research and Innovation Programme (NANOPHOM, grant agreement no. 715832). J.M.M.-M. acknowledges funding from the Spanish Ministry of Education and Vocational Training through an FPU programme under grant FPU14/00890. The project that gave rise to these results received the support of a fellowship granted to V.E. from "la Caixa" Foundation (ID 100010434). The fellowship code is LCF/BQ/ES15/10360025.

Conflict of Interest

The authors declare no conflict of interest.

Keywords

angular distribution, finite size effects, Mie scattering, Monte Carlo, optical disorder, random optical media

Received: July 16, 2019
Revised: October 1, 2019
Published online: November 19, 2019

[1] M. B. van der Mark, M. P. van Albada, A. Lagendijk, *Phys. Rev. B* **1987**, *37*, 3575.
[2] M. P. van Albada, B. A. van Tiggelen, A. Lagendijk, A. Tip, *Phys. Rev. Lett.* **1991**, *66*, 3132.
[3] D. S. Wiersma, M. P. van Albada, A. Ladendijk, *Phys. Rev. Lett.* **1995**, *75*, 1739.
[4] D. S. Wiersma, P. Bartolini, A. Lagendijk, R. Righini, *Nature* **1997**, *390*, 671.
[5] P. M. Johnson, B. P. J. Bret, J. G. Rivas, J. J. Kelly, A. Lagendijk, *Phys. Rev. Lett.* **2002**, *89*, 243901.
[6] I. M. Vellekoop, A. Lagendijk, A. P. Mosk, *Nat. Photonics* **2010**, *4*, 320.
[7] O. L. Muskens, J. G. Rivas, R. E. Algra, E. P. A. M. Bakkers, A. Lagendijk, *Nano Lett.* **2008**, *8*, 2638.
[8] O. L. Muskens, S. L. Diedenhofen, B. C. Kaas, R. E. Algra, E. P. A. M. Bakkers, J. G. Rivas, A. Lagendijk, *Nano Lett.* **2009**, *9*, 930.
[9] J. Aulbach, B. Gjonaj, P. M. Johnson, A. P. Mosk, A. Lagendijk, *Phys. Rev. Lett.* **2011**, *106*, 103901.
[10] J. Bertolotti, E. G. van Putten, C. Blum, A. Lagendijk, W. L. Vos, A. P. Mosk, *Nature* **2012**, *491*, 232.
[11] A. Cazé, R. Pierrat, R. Carminati, *Photonics Nanostruct.: Fundam. Appl.* **2012**, *10*, 339.
[12] A. P. Mosk, A. Lagendijk, G. Lerosey, M. Fink, *Nat. Photonics* **2012**, *6*, 283.
[13] D. S. Wiersma, *Nat. Photonics* **2013**, *7*, 188.
[14] M. Reufer, L. F. Rojas-Ochoa, S. Ko, J. J. Saens, F. Scheffold, *Appl. Phys. Lett.* **2007**, *91*, 171904.
[15] P. D. García, R. Sapienza, J. Bertolotti, M. D. Martín, Á. Blanco, A. Altube, L. Viña, D. S. Wiersma, C. López, *Phys. Rev. A* **2008**, *78*, 023823.
[16] J. Bertolotti, K. Vynck, L. Pattelli, P. Barthelemy, S. Lepri, D. S. Wiersma, *Adv. Funct. Mater.* **2010**, *20*, 965.
[17] P. D. García, R. Sapienza, C. López, *Adv. Mater.* **2010**, *22*, 12.
[18] J. M Miranda-Muñoz, G. Lozano, H. Míguez, *Adv. Opt. Mater.* **2017**, *5*, 1700025.
[19] L. E. McNeil, R. H. French, *Acta Mater.* **2000**, *48*, 4571.
[20] S. M. Luke, B. T. Hallam, P. Vukusic, *Appl. Opt.* **2010**, *49*, 4246.

[21] M. Burresi, L. Cortese, L. Pattelli, M. Kolle, P. Vukusic, D. S. Wiersma, U. Steiner, S. Vignolini, *Sci. Rep.* **2014**, *4*, 6075.
[22] S. Caixeiro, M. Peruzzo, O. D. Onelli, S. Vignolini, R. Sapienza, *ACS Appl. Mater. Interfaces* **2017**, *9*, 7885.
[23] J. Syurik, G. Jacucci, O. D. Onelli, H. Hölscher, S. Vignolini, *Adv. Funct. Mater.* **2018**, *28*, 1706901.
[24] M. S. Toivonen, O. D. Onelli, G. Jacucci, V. Lovikka, O. J. Rojas, O. Ikkala, S. Vignolini, *Adv. Mater.* **2018**, *30*, 1704050.
[25] B. T. Hallam, A. G. Hiorns, P. Vukusic, *Appl. Opt.* **2009**, *48*, 3243.
[26] P. D. García, R. Sapienza, L. S. Froufe-Pérez, C. López, *Phys. Rev. B* **2009**, *79*, 241109.
[27] P. D. García, R. Sapienza, C. Toninelli, C. López, D. S. Wiersma, *Phys. Rev. A* **2011**, *84*, 023813.
[28] F. E. Gálvez, P. R. F. Barnes, J. Halme, H Míguez, *Energy Environ. Sci.* **2014**, *7*, 689.
[29] A. Jiménez-Solano, J. Delgado-Sánchez, M. E. Calvo, J. M. Miranda-Muñoz, G. Lozano, D. Sancho, E. Sánchez-Cortezón, H. Míguez, *Prog. Photovolt: Res. Appl.* **2015**, *23*, 1785.

